

Modeling and Stability Analysis of a DC Microgrid Employing Distributed Control Algorithm

Niloofer Ghanbari¹, M. Mobarrez², and S. Bhattacharya¹

¹Department of Electrical and Computer Engineering
North Carolina State University, Raleigh, NC, USA

²ABB Corporate Research Center, Raleigh, NC, USA

Abstract—DC microgrids have higher efficiency, reliability and lower costs compared to the AC systems due to linking DC loads to the DC sources and reducing conversion stages. Thus, they are gaining more and more popularity and the interest in DC microgrids is increasing. In this paper, we are deriving mathematical model of a DC microgrid consisting of photovoltaic (PV) arrays, Battery Energy Storage Systems (BESS) and grid-tied converter, employing distributed control algorithm. The core structure of this work is mathematical modeling of all converters in the discussed microgrid with their voltage, current and droop controllers. Then, the stability analysis for the system and its control algorithm is performed to ensure the stability of DC microgrid in all operating modes. Finally, MATLAB/Simulink is used for demonstrating the capability of the mathematical model in modeling the DC microgrid and its control algorithm.

Index Terms—DC Microgrid, Distributed Control Algorithm, Power Balancing, Droop Control Method, Stability Analysis, State Space Modeling.

I. INTRODUCTION

Renewable-based sources can be connected to the grid through power electronic converters or to be combined with local loads and BESS to form an independent power system (microgrid) [1]. While remarkable progress has been made in improving the performance of AC microgrids, DC microgrids have also been recognized as an attractive option for many applications because of their higher efficiency, higher reliability, improved stability, more natural interface to many types of renewable energy sources and energy storage systems, and better compliance with modern consumer loads [2] - [5].

One of the challenges associated with employing DC microgrids, is to implement a reliable control algorithm that ensures all the power converters maintain stable DC bus voltage and power sharing is achieved among them [6].

To address the mentioned challenge, various droop based control methods have been proposed [7]. Voltage droop control method is a well known method in DC microgrids, where the reference voltage of each source is calculated using its nominal output voltage, output current and a droop coefficient. In a parallel system utilizing droop controller, the output power of each source is proportional to its droop coefficient [2].

In this method, the stability is commonly obtained by sources in parallel controlling the bus voltage cooperatively. Therefore, it is necessary to have an accurate model of the system, including the converters and the control algorithm, for stability

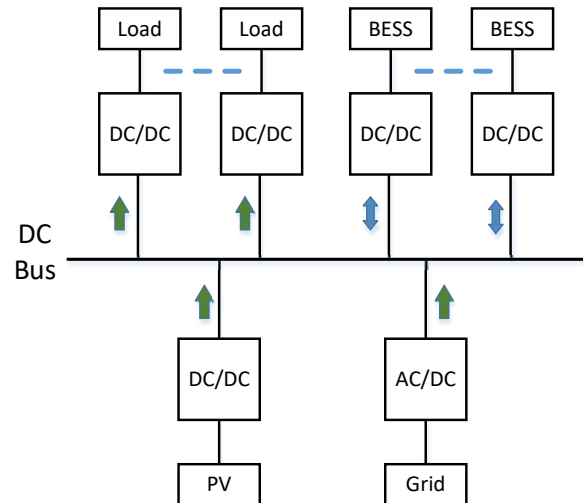


Fig. 1: Schematic of a typical DC microgrid.

analysis when designing the controller. The core structure of this work is deriving mathematical model of all the converters and their controllers in the microgrid shown in Fig. 1. Then, to use this model for the stability analysis of DC microgrid.

In order to model the DC microgrid with all sources and their converters, the state space model is utilized. The state space description is a well known method for describing a system in terms of mathematical model. As the system has multiple modes of operation, the mathematical model is derived for each mode and the stability is examined by observing eigenvalues of the model.

The remainder of this paper is organized as following. Section II explains the distributed control algorithm employed in the DC microgrid. This control algorithm will be used for the model derivation in the next section. In section III, mathematical models of the system are derived and discussed for different operation modes. Next, in section IV, stability analysis is performed to ensure the stability of the system in all operating modes. Simulation of the model is done in MATLAB/Simulink in Section V for demonstrating the capability of the mathematical model in modeling the DC microgrid and its control algorithm. Finally, section VI concludes the paper.

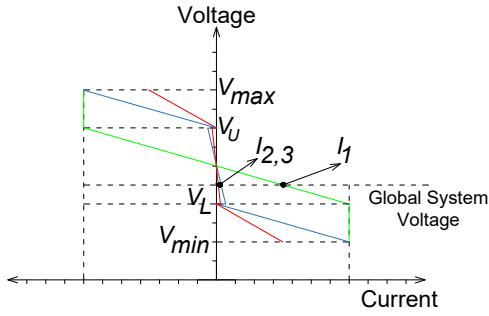


Fig. 2: V-I characteristic of slack terminals.

II. EMPLOYED CONTROL ALGORITHM

The control algorithm employed for the microgrid shown in Fig. 1 is similar to what authors proposed in [2]. The basis of the control platform is to achieve stability by paralleling voltage sources on the DC bus.

It is specified that each source is able to regulate the voltage at its output. Each source is designed with the knowledge of its topology, switches, power source, and output capacitance such that it is stable under any external load fluctuations within the limits of its power rating. It is a 'slack' source, similar to slack generators in power systems, in that it provides whatever power is necessary to ensure power balance and maintain the bus voltage. As a system expands to include multiple sources, the system is stable as long as each source is stable.

Fig. 2 shows the I-V characteristics of the slack sources of the system and how the global system voltage is determined by the balance of load and supply. Each converter in the system, measures the DC bus voltage and sets its mode accordingly. The voltage levels are defined as following

$$\begin{cases} V_{min} = 365v \\ V_L = 372.5v \\ V_U = 387.5v \\ V_{max} = 395v \end{cases} \quad (1)$$

As it can be seen in Fig. 2, there are two modes of operation for the DC microgrid based on the DC bus voltage. The following explains these two modes in details.

Mode I ($V_L < V_{dc} < V_U$): In this mode, all three voltage sources (BESSs and grid-tied converter) are operating in droop control mode. In the other words, all three converters are contributing in voltage regulation. However, the droop coefficient of BESS are set higher than the grid-tied converter so the majority of power comes from the grid-tied converter. Meaning that the grid-tied converter is the primary source responsible for regulating the DC bus voltage and BESS are the backup sources.

$$\begin{cases} V_L < V_{dc} < V_U : \\ V_{Grid}^* = 380 - R_{dG} * I_G \\ V_{BESS}^* = 380 - 1.5 * I_B \\ R_{dG} = \frac{15}{260} \end{cases} \quad (2)$$

where, R_{dG} is the droop coefficient of the grid-tied converter. As it can be seen, in this mode, droop coefficients for BESSs are considered 30 times of the grid-tied converter droop coefficient.

Mode II ($V_{dc} > V_U$ or $V_{dc} < V_L$): In this mode, grid-tied converter is operating in current control mode and acts as a current source/sink. This happens when the grid-tied converter cannot meet the demand and voltage falls out of the dead-band ($V_{dc} > V_U$ or $V_{dc} < V_L$). BESSs remain in droop control mode and update their droop coefficient to a lower amount so they can operate as the slack terminals.

$$\begin{cases} V_{dc} > V_U : V_{BESS}^* = 387.5 - R_{dB} * I_B \\ V_{dc} < V_L : V_{BESS}^* = 372.5 - R_{dB} * I_B \\ R_{dB} = \frac{7.5}{65} \end{cases} \quad (3)$$

where, R_{dB} is the droop coefficient of BESS.

As it can be seen, in this mode, droop coefficients for BESSs are considered less than Mode I.

It should be mentioned that in all above expressions, currents injected to the DC bus are considered as positive and the currents drawn from the microgrid are considered negative.

The outer control layer (droop control) discussed above, handles the energy management in the microgrid. However, there shall be inner voltage and current control layers to ensure stability of the individual converters in the transients. Block diagram of a given converter and its all control layers including: droop controller, voltage and current controllers are shown in Fig. 3.

In modeling the sources with their controllers, the battery converters are considered as bi-directional buck converters and the grid-tied converter is assumed to be a double stage converter (a two-level voltage source inverter in series with a bi-directional converter). The first stage of the grid-tied converter, voltage source inverter (VSI), considered to be fast enough so that the internal DC bus voltage of the converter, the input voltage of the second stage, is kept constant. With these assumptions, both of the grid-tied converter and BESS are modeled as the bi-directional buck converters. And therefore, their controllers are designed similarly.

Moreover, PV arrays are considered to operate in Maximum Power Point Tracking (MPPT) and can be considered a variable current source. In the same manner, loads can be considered as variable current sink.

III. MATHEMATICAL MODEL

Fig. 3 shows the average model of the buck converter and its controllers. As it can be seen from this figure, the voltage and current controllers are considered as PI controllers. Using this figure, we can obtain the mathematical model of the DC microgrid. As mentioned earlier, the PV arrays work at MPPT so they are considered as variable current sources and loads are considered as variable current sinks. Thus, the control algorithm discussed in the previous section is utilized only for BESSs and grid-tied converter, i.e. the 'slack' terminals.

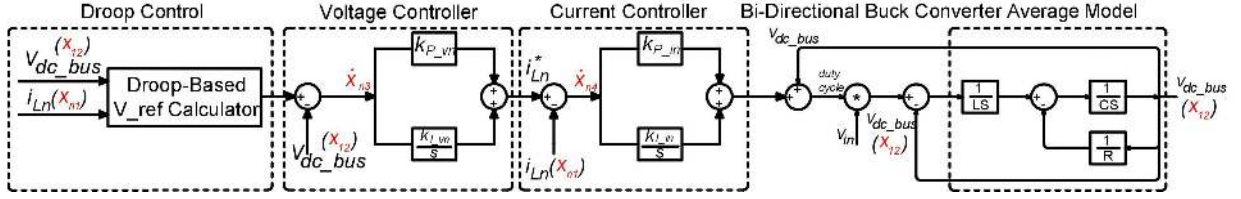


Fig. 3: Control block diagram of a single converter.

TABLE I: States definition for the voltage sources of the system.

State Variable	Description
x_{n1}	Inductor Current of n^{th} converter
x_{12}	Output Capacitor Voltage of first converter
x_{n3}	Output of the Voltage Controller Intergrator
x_{n4}	Output of the Current Controller Intergrator

In this section, state space modeling method is used to model the DC microgrid. The state space description is a well known method for describing a system in terms of mathematical model. As the system has multiple modes of operation, the mathematical model shall be derived for each modes of operation and the stability in each mode shall be discussed.

First step in state space modeling is defining the state variables. We can define the state variables as in Table I. Also, these state variables are shown in the block diagram of Fig. 3.

By considering state space model and examining the eigenvalues of matrix A, one can find if the system is stable or not. First, the mathematical model for Mode I is derived in which all the converters operate in droop control mode. Then, this general model will be used for obtaining the model for Mode II.

For a single converter operating in droop control mode, the following equations can be obtained from Fig. 3, with the states defined in Table I.

$$\dot{x}_{13} = V_{nom} - R_{d1}x_{11} - x_{12} \quad (4)$$

where, R_{d1} is the droop control coefficient for the first converter and V_{nom} is the nominal voltage of the converter. Then, x_{14} can be described as following

$$\begin{aligned} \dot{x}_{14} &= k_{P_{v1}}[V_{nom} - R_{d1}x_{11} - x_{12}] + k_{I_{v1}}x_{13} - x_{11} \\ &= (-1 - k_{P_{v1}}R_{d1})x_{11} - k_{P_{v1}}x_{12} + k_{I_{v1}}x_{13} + k_{P_{v1}}V_{nom} \end{aligned} \quad (5)$$

where, $k_{P_{v1}}$ and $k_{I_{v1}}$ are the proportional and integral gains for the voltage controller, respectively. Duty cycle D can be written as

$$\begin{aligned} D &= (-k_{P_{i1}} - k_{P_{i1}}k_{P_{v1}}R_{d1})x_{11} - k_{P_{i1}}k_{P_{v1}}x_{12} \\ &\quad + k_{P_{i1}}k_{I_{v1}}x_{13} + k_{I_{i1}}x_{14} + k_{P_{i1}}k_{P_{v1}}V_{nom} \end{aligned} \quad (6)$$

where, $k_{P_{i1}}$ and $k_{I_{i1}}$ are the proportional and integral gains for the current controller, respectively.

From the average model of buck converter, x_{11} is related to D as following

$$\dot{x}_{11} = -\frac{1}{L}x_{12} + \frac{D}{L} + \frac{1}{L}x_{12} = \frac{D}{L} \quad (7)$$

By inserting the obtained D into the Eq. 7

$$\begin{aligned} \dot{x}_{11} &= \frac{-k_{P_{i1}} - k_{P_{i1}}k_{P_{v1}}R_{d1}}{L_1}x_{11} + \frac{-k_{P_{i1}}k_{P_{v1}}}{L_1}x_{12} \\ &\quad + \frac{k_{P_{i1}}k_{I_{v1}}}{L_1}x_{13} + \frac{k_{I_{i1}}}{L_1}x_{14} + \frac{k_{P_{i1}}k_{P_{v1}}V_{nom}}{L_1} \end{aligned} \quad (8)$$

x_{12} indicates the derivative of output voltage and can be found from the following equation.

$$\dot{x}_{12} = \frac{1}{C_1}(x_{11}) - \frac{1}{RC_1}x_{12} \quad (9)$$

where, C_1 is the output capacitor of the first converter.

From Eq. 4 to Eq. 12, the state space model of a single converter and its controllers can be written as

$$\begin{aligned} \begin{bmatrix} \dot{x}_{11} \\ \dot{x}_{12} \\ \dot{x}_{13} \\ \dot{x}_{14} \end{bmatrix} &= \underbrace{\begin{bmatrix} \frac{-k_{P_{i1}} - k_{P_{i1}}k_{P_{v1}}R_{d1}}{L_1} & \frac{-k_{P_{i1}}k_{P_{v1}}}{L_1} & \frac{k_{P_{i1}}k_{I_{v1}}}{L_1} & \frac{k_{I_{i1}}}{L_1} \\ \frac{1}{C_1} & \frac{-1}{RC_1} & 0 & 0 \\ -R_{d1} & -1 & 0 & 0 \\ -1 - k_{P_{v1}}R_{d1} & -k_{P_{v1}} & k_{I_{v1}} & 0 \end{bmatrix}}_A \\ &\quad + \underbrace{\begin{bmatrix} \frac{V_{in1}}{L_1}(k_{P_{i1}}k_{P_{v1}}) \\ 0 \\ 1 \\ k_{P_{v1}} \end{bmatrix}}_B V_{nom} \end{aligned} \quad (10)$$

This state space model is for the case that the output current of the converter, I_{Ln} is positive. Meaning that the load is greater than PV (under generation).

In order to demonstrate the effect of PV over generation in the modeling, the feedback current in Fig. 3, I_{Ln} , can be written as $I_{load} - I_{pv}$. By doing this, the state space model of converter

TABLE II: Specifications of the DC Microgrid.

Component	Power Rating	Max Current	Nominal Output Voltage	Output LC Filter	Switching Frequency
Grid-Tied Converter	60kW	130(A)	380V _{dc}	$L = 5mH, C = 500\mu F$	20kHz
BESS Units (each)	30kW	65(A)	380V _{dc}	$L = 5mH, C = 500\mu F$	20kHz
PV Arrays	80kW	220(A)	380V _{dc}	$L = 5mH, C = 500\mu F$	20kHz
Load	50kW	137(A)	380V _{dc}	$L = 5mH, C = 500\mu F$	20kHz

can be rewritten as

$$\begin{aligned}
 \begin{bmatrix} \dot{x}_{11} \\ \dot{x}_{12} \\ \dot{x}_{13} \\ \dot{x}_{14} \end{bmatrix} &= \underbrace{\begin{bmatrix} \frac{-k_{P_{i1}} - k_{P_{i1}} k_{P_{v1}} R_{d1}}{L_1} & \frac{-k_{P_{i1}} k_{P_{v1}}}{L_1} & \frac{k_{P_{i1}} k_{I_{v1}}}{L_1} & \frac{k_{I_{i1}}}{L_1} \\ \frac{1}{C_1} & \frac{R_{d1}}{C_1} & 0 & 0 \\ -R_{d1} & -1 & 0 & 0 \\ -1 - k_{P_{v1}} R_{d1} & -k_{P_{v1}} & k_{I_{v1}} & 0 \end{bmatrix}}_A \\
 &+ \underbrace{\begin{bmatrix} \frac{V_{in1}}{L_1} (k_{P_{i1}} k_{P_{v1}}) \\ 0 \\ 1 \\ k_{P_{v1}} \end{bmatrix}}_{B_1} V_{nom} - \underbrace{\begin{bmatrix} \frac{-k_{P_{i1}} - k_{P_{i1}} k_{P_{v1}} R_{d1}}{L_1} \\ \frac{1}{C_1} \\ -R_{d1} \\ -1 - k_{P_{v1}} R_{d1} \end{bmatrix}}_{B_2} I_{pv}
 \end{aligned} \quad (11)$$

It can be seen that matrix A remains unchanged for positive and negative currents. Thus, it can be said that the stability of the system is independent of PV generation. Therefore, the PV over generation is not considered in the modeling.

The obtained model of a single converter can be used for a DC microgrid with multiple voltage sources in parallel. Table I shows the state variables of a microgrid with n parallel converters. It can be seen that x_{12} , the output voltage of first converter, is the common state. Meaning that the output voltages of all paralleled converters are equal and there is no need to define this state for the other converters.

Using the state space description of single compensated converter, the model of DC microgrid with three voltage sources operating in Mode I can be obtained. All the state variables are independent except the common state which can be written as

$$\dot{x}_{12} = \frac{1}{C_1 + C_2 + C_3} (x_{11} + x_{21} + x_{31}) - \frac{1}{R(C_1 + C_2 + C_3)} x_{12} \quad (12)$$

where, C_1 , C_2 and C_3 are the output capacitors of the first, second and third converter, respectively.

The state space model of the DC microgrid in Mode I of is shown in the Appendix.

Using the general mode of Mode I, the state space model for Mode II of operation can be obtained. Model of DC microgrid in this mode is shown in Appendix.

Matrix A of the derived state space models can be used to evaluate the stability of the system.

IV. STABILITY ANALYSIS

The stability of system can be determined by examining the eigenvalues of the state transition matrix (A matrix). The system is asymptotically stable if all the eigenvalues of the transition matrix are negative. In an asymptotically stable

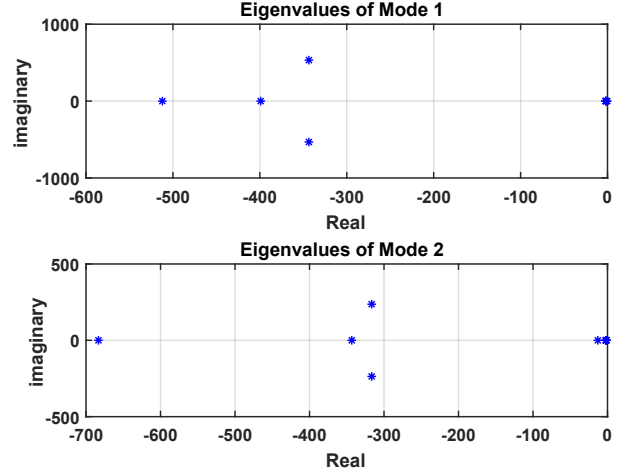


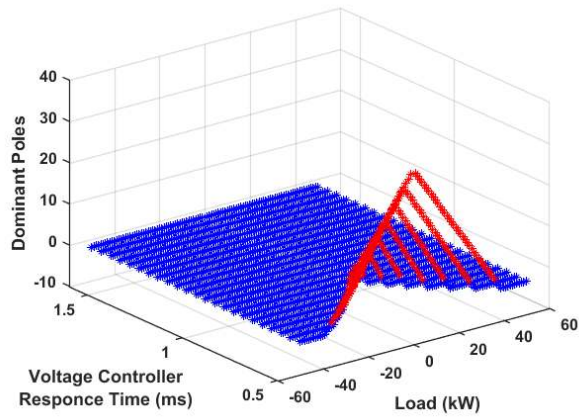
Fig. 4: Real and Imaginary parts of eigenvalues for Mode I and Mode II.

system, the system will always return to an equilibrium. The models developed for the DC system in different operation modes in the previous section, are used for stability analysis of the DC microgrids with the specifications shown in Table II. And the eigenvalues of the system are plotted in Fig. 4 for two specific operation points. Fig. 4 shows real and imaginary parts of eigenvalues for two specific operation points. As it can be seen, all of the eigenvalues have negative real parts, which means the system is stable.

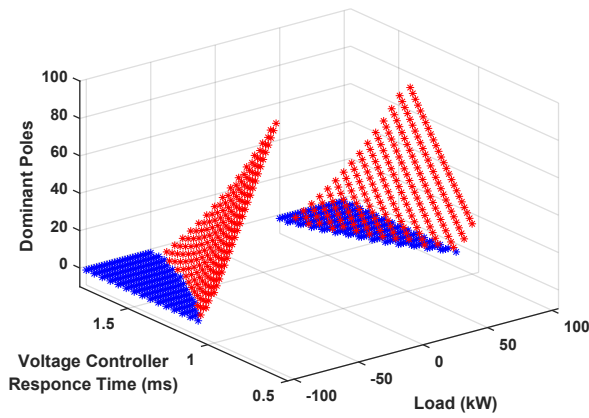
Results shown in Fig. 4 are for two specific operating points. In order to prove the stability for all loading conditions, we should monitor the eigenvalues with the change of load power. Moreover, it is necessary to find the stable region with respect to the controller response times. For this purpose, different loading conditions and different voltage controller response time are considered. Then, the real part of dominant eigenvalues of the system are plotted. The stable/unstable operating regions of the system are shown in Fig. 5.

It should be noted that the current controller response time shall be faster than the response time of the voltage controller for stability. Thus, in this simulations, the response time of the current controller is considered at least 5 times of the response time of voltage controller.

In Fig. 5, the red dots show positive poles and unstable regions of the system in mode I and II. By observing the figure, we find that in order to have a stable system for all loading operations, appropriate response time for the voltage controller should be considered.



(a) Mode I.



(b) Mode II.

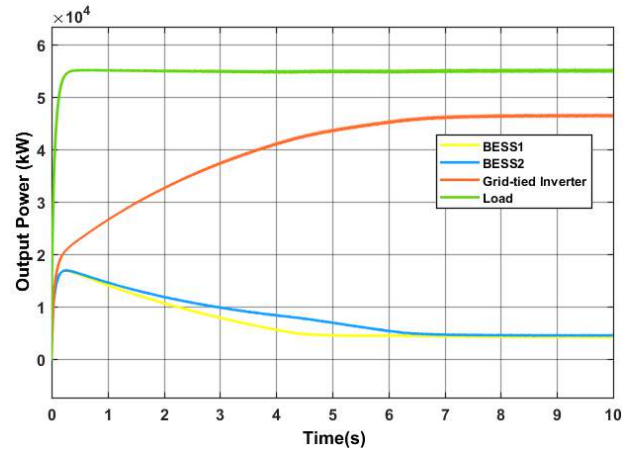
Fig. 5: Stable/unstable operating regions in different loading conditions and different voltage controller response times.

V. SIMULATION RESULTS

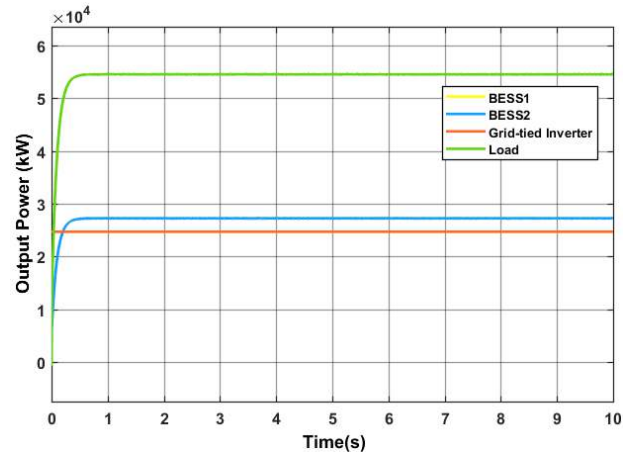
In order to demonstrate the capability of the mathematical model in modeling the DC microgrid and its control algorithm, the derived state space model of the DC microgrid is simulated in MATLAB/Simulink. Simulation results for Mode I and Mode II are summarized in Fig. 6a and 6b, respectively. As it can be seen in Fig 6a, in Mode I of operation the grid-tied converter is regulating the DC bus voltage by providing the required power and BESSs are at stand by due to the difference between their droop coefficients.

The same analysis can be done for the results shown in Fig. 6b. In this figure, for Mode II, the BESSs are regulating the DC bus voltage by providing the required power and grid-tied converter is at stand by. The results of the simulation show that the mathematical model is capable to model the DC microgrid and its controller.

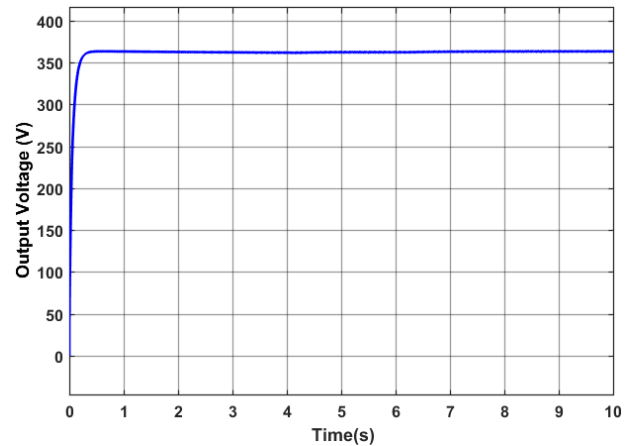
Moreover, in Fig. 6c, we can see that the DC bus voltage remains in the desired range of output voltage as defined in Eq. 1.



(a)



(b)



(c)

Fig. 6: (a) Output power of BESS and grid-tied inverter in Mode I. (b) Output power of BESS and grid-tied inverter in Mode II. (c) DC bus voltage.

VI. CONCLUSION

DC microgrids have higher efficiency, reliability and lower costs compared to the AC systems due to linking DC loads to the DC sources and reducing conversion stages. Thus, they

are gaining more and more popularity. In this paper, the mathematical models of all converters in the DC microgrid with their voltage, current and droop controllers has been derived. Then, the stability analysis for the system and its control algorithm is performed to ensure the stability of DC microgrid in all operating modes. Finally, MATLAB/Simulink is used for demonstrating the capability of the mathematical model in modeling the DC microgrid and its control algorithm.

REFERENCES

- [1] R. H. Lasseter. "Microgrids." IEEE Power Engineering Society Winter Meeting. vol. 1, pp. 305-308. 2002.
- [2] M. Mobarrez, D. Fregosi, Gh. Jalali, S. Bhattacharya, and M.A. Bahmani, "A novel control method for preventing the PV and load fluctuations in a DC microgrid from transferring to the AC power grid", DC Microgrids (ICDCM), 2017 IEEE Second International Conference, Germany, Aug 2017.
- [3] M. Mobarrez, S. Bhattacharya, and D. Fregosi, "Implementation of distributed power balancing strategy with a layer of supervision in a low-voltage DC microgrid", Applied Power Electronics Conference and Exposition (APEC), Tampa, USA, March 2017.
- [4] Z. Mahmoodzadeh, N. Ghanbari, A. Mehrizi-sani, M. Ehsan; "Energy Loss Estimation in Distribution Networks Using Stochastic Simulation", Power and Energy Society General Meeting, IEEE, July 2015, Denver, USA.
- [5] M. Mobarrez, D. Fregosi, S. Bhattacharya, and M.A. Bahmani, "Grounding architectures for enabling ground fault ride-through capability in DC microgrids", DC Microgrids (ICDCM), 2017 IEEE Second International Conference, Germany, Jun 2017.
- [6] X. Lu, K. Sun, J. M. Guerrero, and Juan C. Vasquez, "Stability Enhancement Based on Virtual Impedance for DC Microgrids With Constant Power Loads", IEEE Transaction on Smart Grid, Nov. 2015.
- [7] B.T. Irving, and M.M. Jovanovic, "Analysis, design, and performance evaluation of droop current-sharing method", Applied Power Electronics Conference and Exposition (APEC), Los Angeles USA, Feb. 2000.
- [8] D. Boroyevich, I. Cvetkovic, D. Dong, R. Burgos, F. Wang, and F. Lee, "Future electronic power distribution systems a contemplative view", in Proc. 12th Int. Conf. Optimization Electr. Electron. Equipment, May 2010.
- [9] D. Giaouris, S. Banerjee, B. Zahawi, and V. Pickert, "Stability analysis of the continuous-conduction-mode buck converter via filippov's method", IEEE Transactions on Circuits and Systems-I, May 2008.
- [10] D. Giaouris, A. Elbkosh, V. Pickert, B. Zahawi, and S. Banerjee, "Control of period doubling bifurcation in dc-dc converters", International Control Conference (ICC2006), Glasgow UK, 2006.
- [11] D. Giaouris, A. Elbkosh, V. Pickert, B. Zahawi, and S. Banerjee, "Control of period doubling bifurcation in dc-dc converters", International Control Conference (ICC2006), Glasgow UK, 2006.
- [12] K. Asadi, H. Ramshankar, H. Pullagurla, A. Bhandare, S. Shanbhag, P. Mehta, S. Kundu, S., K. Han, E. Lobaton, and T. Wu, "Building an Integrated Mobile Robotic System for Real-time Applications in Construction." arXiv preprint arXiv:1803.01745.
- [13] H. M. Bagherpoor, and F. R. Salmasi, "Robust Model Reference Adaptive Output Feedback Tracking for Uncertain Linear Systems with Actuator Fault Based on Reinforced Dead-zone Modification", ISA Transactions Journal, vol. 57, pp. 51-56, 2015.

VII. APPENDIX

Model of the system in Mode I:

$$\begin{bmatrix} \dot{x}_{11} \\ \dot{x}_{12} \\ \dot{x}_{13} \\ \dot{x}_{14} \\ \dot{x}_{21} \\ \dot{x}_{23} \\ \dot{x}_{24} \\ \dot{x}_{31} \\ \dot{x}_{33} \\ \dot{x}_{34} \end{bmatrix} = \begin{bmatrix} a_{11} & a_{12} & a_{13} & a_{14} & 0 & 0 & 0 & 0 & 0 & 0 & 0 \\ a_{21} & a_{22} & 0 & 0 & a_{25} & 0 & 0 & a_{28} & 0 & 0 & 0 \\ -R_{d1} & -1 & 0 & 0 & 0 & 0 & 0 & 0 & 0 & 0 & 0 \\ a_{41} & a_{42} & a_{43} & 0 & 0 & 0 & 0 & 0 & 0 & 0 & 0 \\ 0 & a_{52} & 0 & 0 & a_{55} & a_{56} & a_{57} & 0 & 0 & 0 & 0 \\ 0 & -1 & 0 & 0 & -R_{d2} & 0 & 0 & 0 & 0 & 0 & 0 \\ 0 & a_{72} & 0 & 0 & a_{75} & a_{76} & 0 & 0 & 0 & 0 & 0 \\ 0 & a_{82} & 0 & 0 & 0 & 0 & 0 & a_{88} & a_{89} & a_{810} & 0 \\ 0 & -1 & 0 & 0 & 0 & 0 & 0 & -R_{d3} & 0 & 0 & 0 \\ 0 & a_{102} & 0 & 0 & 0 & 0 & 0 & a_{108} & a_{109} & 0 & 0 \end{bmatrix} \begin{bmatrix} x_{11} \\ x_{12} \\ x_{13} \\ x_{14} \\ x_{21} \\ x_{23} \\ x_{24} \\ x_{31} \\ x_{33} \\ x_{34} \end{bmatrix} + \begin{bmatrix} \frac{k_{P_{i1}}k_{P_{v1}}}{L_1} \\ 0 \\ 1 \\ k_{P_{v1}} \\ \frac{k_{P_{i2}}k_{P_{v2}}}{L_2} \\ 1 \\ k_{P_{v2}} \\ \frac{k_{P_{i3}}k_{P_{v3}}}{L_3} \\ 1 \\ k_{P_{v3}} \end{bmatrix} V_{nom} \quad (13)$$

$$\begin{aligned} a_{11} &= \frac{-k_{P_{i1}} - k_{P_{i1}}k_{P_{v1}}R_{d1}}{L_1} & a_{12} &= \frac{-k_{P_{i1}}k_{P_{v1}}}{L_1} & a_{13} &= \frac{k_{P_{i1}}k_{I_{v1}}}{L_1} \\ a_{14} &= \frac{k_{I_{i1}}}{L_1} & a_{21} &= \frac{1}{C_1 + C_2 + C_3} & a_{22} &= \frac{-1}{R(C_1 + C_2 + C_3)} \\ a_{25} &= a_{28} = \frac{1}{C_1 + C_2 + C_3} & a_{41} &= -1 - k_{P_{v1}}R_{d1} & a_{42} &= -k_{P_{v1}} \\ a_{43} &= k_{I_{v1}} & a_{52} &= \frac{-k_{P_{i2}}k_{P_{v2}}}{L_2} & a_{55} &= \frac{-k_{P_{i2}} - k_{P_{i2}}k_{P_{v2}}R_{d2}}{L_2} \\ a_{56} &= \frac{k_{P_{i2}}k_{I_{v2}}}{L_2} & a_{57} &= \frac{k_{I_{i2}}}{L_2} & a_{72} &= -k_{P_{v2}} \\ a_{75} &= -1 - k_{P_{v2}}R_{d2} & a_{76} &= k_{I_{v2}} & a_{82} &= \frac{-k_{P_{i3}}k_{P_{v3}}}{L_3} \\ a_{88} &= \frac{-k_{P_{i3}} - k_{P_{i3}}k_{P_{v3}}R_{d3}}{L_3} & a_{89} &= \frac{k_{P_{i3}}k_{I_{v3}}}{L_3} & a_{810} &= \frac{k_{I_{i3}}}{L_3} \\ a_{102} &= -k_{P_{v3}} & a_{108} &= -1 - k_{P_{v3}}R_{d3} & a_{109} &= k_{I_{v3}} \end{aligned}$$

Model of the system in Mode II:

$$\begin{bmatrix} \dot{x}_{11} \\ \dot{x}_{12} \\ \dot{x}_{14} \\ \dot{x}_{21} \\ \dot{x}_{23} \\ \dot{x}_{24} \\ \dot{x}_{31} \\ \dot{x}_{33} \\ \dot{x}_{34} \end{bmatrix} = \begin{bmatrix} b_{11} & b_{12} & b_{13} & 0 & 0 & 0 & 0 & 0 & 0 & 0 \\ b_{21} & b_{22} & 0 & b_{24} & 0 & 0 & b_{27} & 0 & 0 & 0 \\ -1 & 0 & 0 & 0 & 0 & 0 & 0 & 0 & 0 & 0 \\ 0 & b_{42} & 0 & b_{44} & b_{45} & b_{46} & 0 & 0 & 0 & 0 \\ 0 & -1 & 0 & -R_{d2} & 0 & 0 & 0 & 0 & 0 & 0 \\ 0 & b_{62} & 0 & b_{64} & b_{65} & 0 & 0 & 0 & 0 & 0 \\ 0 & b_{72} & 0 & 0 & 0 & 0 & b_{77} & b_{78} & b_{79} & 0 \\ 0 & -1 & 0 & 0 & 0 & 0 & -R_{d3} & 0 & 0 & 0 \\ 0 & b_{92} & 0 & 0 & 0 & 0 & b_{97} & b_{98} & 0 & 0 \end{bmatrix} \begin{bmatrix} x_{11} \\ x_{12} \\ x_{14} \\ x_{21} \\ x_{23} \\ x_{24} \\ x_{31} \\ x_{33} \\ x_{34} \end{bmatrix} + \begin{bmatrix} 0 \\ 0 \\ 0 \\ \frac{k_{P_{i2}}k_{P_{v2}}}{L_2} \\ 1 \\ k_{P_{v2}} \\ \frac{k_{P_{i3}}k_{P_{v3}}}{L_3} \\ 1 \\ k_{P_{v3}} \end{bmatrix} V_{nom} \quad (14)$$

$$\begin{aligned} b_{11} &= -\frac{k_{P_{i1}}}{L_1} & b_{12} &= 0 & b_{13} &= \frac{k_{I_{i1}}}{L_1} \\ b_{21} &= \frac{1}{C_1 + C_2 + C_3} & b_{22} &= \frac{-1}{R(C_1 + C_2 + C_3)} & b_{24} &= \frac{1}{C_1 + C_2 + C_3} \\ b_{27} &= \frac{1}{C_1 + C_2 + C_3} & b_{42} &= \frac{-k_{P_{i2}}k_{P_{v2}}}{L_2} & b_{44} &= \frac{-k_{P_{i2}} - k_{P_{i2}}k_{P_{v2}}R_{d2}}{L_2} \\ b_{45} &= \frac{k_{P_{i2}}k_{I_{v2}}}{L_2} & b_{46} &= \frac{k_{I_{i2}}}{L_2} & b_{62} &= -k_{P_{v2}} \\ b_{64} &= -1 - k_{P_{v2}}R_{d2} & b_{65} &= k_{I_{v2}} & b_{72} &= \frac{-k_{P_{i3}}k_{P_{v3}}}{L_3} \\ b_{77} &= \frac{-k_{P_{i3}} - k_{P_{i3}}k_{P_{v3}}R_{d3}}{L_3} & b_{78} &= \frac{k_{P_{i3}}k_{I_{v3}}}{L_3} & b_{79} &= \frac{k_{I_{i3}}}{L_3} \\ b_{92} &= -k_{P_{v3}} & b_{97} &= -1 - k_{P_{v3}}R_{d3} & b_{98} &= k_{I_{v3}} \end{aligned}$$